metals

MDPI

Article

Preparation of Spherical Mo_5Si_3 Powder by Inductively Coupled Thermal Plasma Treatment

Jang-Won Kang [1,2], Jong Min Park [1], Byung Hak Choe [2], Seong Lee [3], Jung Hyo Park [3], Ki Beom Park [1], Hyo Kyu Kim [1], Tae-Wook Na [1], Bosung Seo [1] and Hyung-Ki Park [1,*]

1 Gangwon Regional Division, Korea Institute of Industrial Technology, Gangneung 25440, Korea; jwkang@kitech.re.kr (J.-W.K.); pjm2639@kitech.re.kr (J.M.P.); hope92430@kitech.re.kr (K.B.P.); khk4529@kitech.re.kr (H.K.K.); arkasa86@kitech.re.kr (T.-W.N.); bs3863@kitech.re.kr (B.S.)

2 Department of Advanced Metal and Materials Engineering, Gangneung-Wonju National University, Gangneung 25457, Korea; cbh@gwnu.ac.kr

3 Agency for Defense Development, Daejeon 34186, Korea; myhome1992@hanmail.net (S.L.); melpjh@hanmail.net (J.H.P.)

* Correspondence: mse03@kitech.re.kr; Tel.: +82-33-649-4016

Received: 28 June 2018; Accepted: 1 August 2018; Published: 3 August 2018

Abstract: A method was developed to fabricate spherical Mo_5Si_3 powder by milling and spheroidizing using inductively coupled thermal plasma. A Mo_5Si_3 alloy ingot was fabricated by vacuum arc melting, after which it was easily pulverized into powder by milling due to its brittle nature. The milled powders had an irregular shape, but after being spheroidized by the thermal plasma treatment, they had a spherical shape. Sphericity was increased with increasing plasma power. After plasma treatment, the percentage of the Mo_3Si phase had increased due to Si evaporation. The possibility of Si evaporation was thermodynamically analyzed based on the vapor pressure of Mo and Si in the Mo_5Si_3 liquid mixture. By this process, spherical Mo silicide powders with high purity could be fabricated successfully.

Keywords: Mo silicide; Mo_5Si_3; spheroidizing; powder; inductively coupled thermal plasma

1. Introduction

Refractory metal-based silicide alloys, which are also referred to as refractory metal in situ composites, currently receive a lot of attention as structural materials for ultrahigh temperature applications [1–3]. Among these materials, Mo silicide-based alloy [4,5] and Nb silicide-based alloy [6,7] have been intensively studied due to their excellent strength, creep resistance and oxidation resistance at ultrahigh temperature. Furthermore, Mo and Nb have a relative low density compared to other refractory metals, such as Ta and W [8].

Mo silicide-based alloys are composed of α-Mo and Mo silicide. Mo silicides are formed of three main phases: Mo_5Si_3, Mo_3Si, and $MoSi_2$ [9]. Of these, Mo_5Si_3 has the highest melting temperature of 2180 °C [10]. Therefore, many studies have evaluated the high-temperature creep and oxidation resistance of Mo_5Si_3.

Unfortunately, Mo silicide-based alloys have low fracture toughness at ambient temperature [11], along with low machinability due to the low thermal conductivity and brittle nature of Mo silicides [12,13]. Therefore, it is difficult to fabricate components of Mo silicide-based alloys by conventional casting and machining methods. In addition, since in the Mo–Si binary system the Mo_3Si phase is in between the Mo solid solution and the Mo_5Si_3 phases, Mo silicide-based alloys composed of Mo and Mo_5Si_3 cannot be fabricated by casting. However, based on the powder metallurgy process, Mo-based silicide alloys, where the microstructures consist of Mo5Si3–Mo3Si and Mo–Mo5Si3–Mo3Si, could be fabricated.

Hence, powder metallurgy processes are an attractive way to fabricate components of Mo silicide-based alloys. Previous studies have attempted to fabricate Mo silicide-based alloys [14,15] and Mo silicide powders [16] by mechanical alloying. However, powders fabricated by mechanical alloying suffer from low productivity and oxygen contamination, as well as an irregular morphology. With regard to sintering, spherical powders are much more favorable than those with irregular shapes, as they offer higher packing density and fluidity [17].

It is therefore necessary to develop a method to fabricate high-purity spherical Mo silicide powders. To our knowledge, there is no previous work on the preparation of Mo silicide powders or pre-alloyed Mo silicide-based alloy powders by inductively coupled thermal plasma processing. Thus, in this study, we fabricated Mo_5Si_3 powders by pulverizing a Mo_5Si_3 ingot, utilizing its brittle nature. To improve the sphericity of the powders, they were spheroidized by an inductively coupled thermal plasma treatment. The effect of the plasma power on the morphology and phase balance of the powders was examined, and the evaporation behavior of Si during plasma treatment was analyzed thermodynamically.

2. Experimental Procedures

Mo_5Si_3 ingots with a chemical composition of 85.06Mo–14.94Si in wt% (62.5Mo–37.5Si in atom%) were fabricated by vacuum arc melting. For vacuum arc melting, the chamber was evacuated to a high vacuum (10^{-5} torr) by oil diffusion pump and then high-purity argon gas was injected into the chamber until the pressure reached 400 torr. The ingot, which was 150 mm long × 75 mm wide × 10 mm high, was cast in a quadrangle-shaped cold copper crucible and its weight was 1100 g. To homogenize the composition, the ingot was remelted five times.

To analyze the chemical composition and oxygen concentration, the center of the ingot was cut to a cylinder 3 mm in diameter and 5 mm in height, and measurements were carried out five times in each sample. The chemical composition of the ingot and powders, as analyzed by inductively coupled plasma mass spectrometry (ICP-MS) (iCAP Q, Thermo Fisher Scientific, Waltham, MA, USA), is given in Table 1. To measure the concentration of Mo and Si in Mo silicide, ICP-MS was carried out following the procedure in [18].

Table 1. Mo and Si concentrations (in wt%) of the ingot and powders after spheroidizing at plasma powers 3–7 kW. The values given in parenthesis refer to standard deviation.

Sample	Power (kW)	Mo (wt%)	Si (wt%)
Ingot	-	85.17 (0.06)	14.83 (0.04)
Powders after Spheroidizing	3	85.70 (0.05)	14.30 (0.03)
	4	85.91 (0.04)	14.09 (0.02)
	5	86.54 (0.05)	13.46 (0.03)
	6	87.45 (0.06)	12.55 (0.04)
	7	88.85 (0.05)	11.15 (0.03)

The oxygen concentration, as analyzed by an inert gas fusion infrared absorption method (LECO, 736 series), is given in Table 2.

Table 2. Oxygen concentrations (in wt%) of the ingot, powders after milling, and powders after spheroidizing at a plasma power of 6 kW. The values given in parenthesis refer to standard deviation.

Samples	Oxygen (wt%)
Ingot	0.003 (0.001)
Powders after Milling	0.172 (0.002)
Powders after Spheroidizing (6 kW)	0.016 (0.001)

For pulverization, two Mo_5Si_3 ingots with a weight of 2200 g were first crushed using a jaw crusher into particles with a size of less than 3 mm. Then, the particles were ball-milled in a stainless-steel container, using tungsten carbide balls with a diameter of 5 mm as milling media. The ball-to-powder ratio was 5:1 by weight and the steel container was purged with high-purity argon to prevent oxygen contamination during ball milling. The milling was performed for 5 h at a rotational speed of 200 rpm. After milling, the powders were sieved to the range of 38–75 μm, because the powders larger than 75 μm were not perfectly spheroidized by the thermal plasma system used in this study.

The sieved powders were spheroidized using an inductively coupled thermal plasma treatment (RFP-10, PLASNIX, Incheon, Korea). To investigate the spheroidizing behavior with respect to plasma power, plasma powers of 3–7 kW were examined. The other parameters were fixed as follows. The plasma oscillation frequency was 13.56 MHz, and the chamber pressure was 80 KPa. The powder carrier and center gas were high-purity argon, with flow rates of 5 and 2 slm (standard liter per minute), respectively. Since the maximum temperature in the chamber almost reaches 10,000 K during plasma processing, the sheath gas was injected along the chamber wall for cooling. The sheath gas was a mixture of argon and helium (argon/helium = 4:1) with a flow rate of 75 slm. To feed the powders into the plasma chamber, a vibrating feeder was used with a feeding rate of 300 g/h.

The morphology of the powders after sieving and spheroidizing was observed by field emission-scanning electron microscopy (FE-SEM, FEI, QUANTA FEG 250, Thermo Fisher Scientific, Waltham, MA, USA) along with energy-dispersive spectrometry (EDS, Octane Elite EDS, EDAX, Mahwah, NJ, USA). To investigate the phase balance, the powders were analyzed using X-ray diffractometry (XRD, Empyrean, PANalytical, Almelo, The Netherlands) with Cu Kα radiation, in the 2θ range of 25–75°. For the XRD analysis, the samples were selected at random. The powder size distribution was investigated using a powder size analyzer (Mastersizer 3000, Malvern Panalytical, Malvern, UK). To understand the Si evaporation behavior during plasma treatment, thermodynamic parameters such as the standard Gibbs free energy change and activity coefficient were calculated by Thermo-Calc using the SSOL database.

3. Results and Discussion

Figure 1 is the microstructure of the cast Mo_5Si_3 ingot observed by back-scattered electron imaging. The ingot was composed of two phases. By EDS analyses, the Si concentrations of the dark area (Point 1) and bright area (Point 2) are 14.28 and 9.15 wt%, respectively, which correspond with the Si concentrations of Mo_5Si_3 and Mo_3Si (14.94 and 8.89 wt%). This result indicates that the dark and bright areas were the Mo_5Si_3 and Mo_3Si phases, respectively.

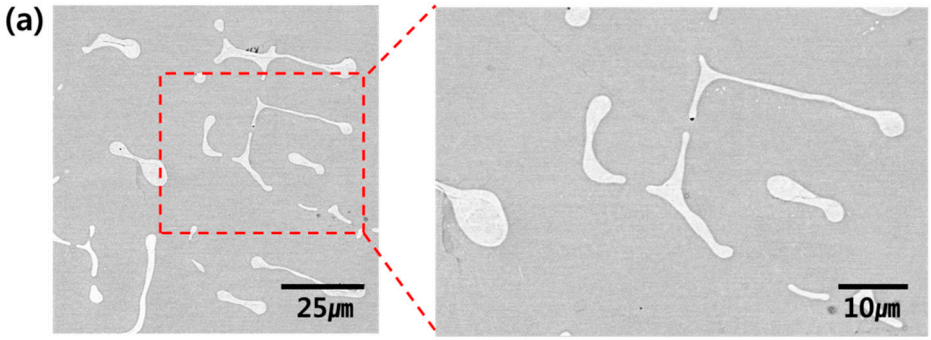

Figure 1. *Cont.*

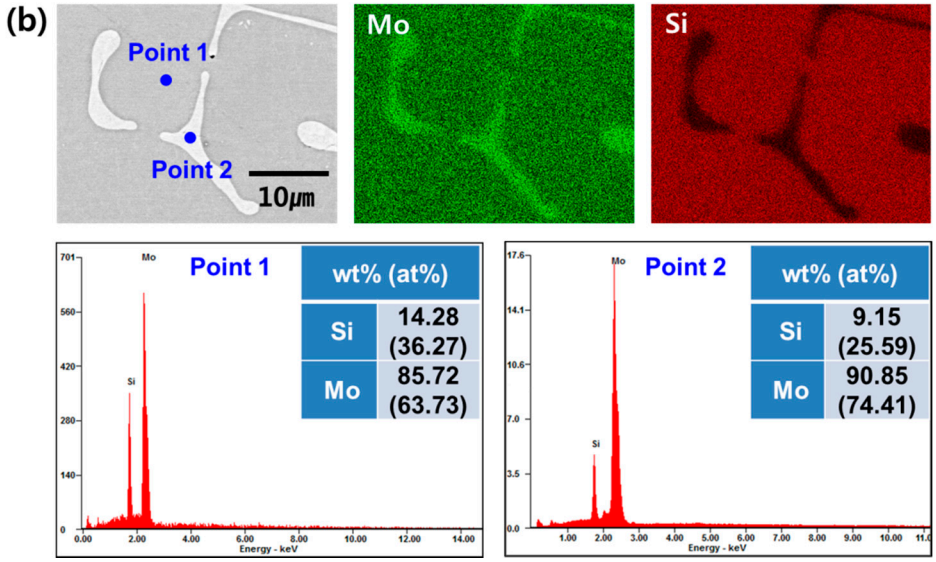

Figure 1. (**a**) The microstructure of the cast Mo_5Si_3 ingot observed by back-scattered electron imaging, and (**b**) EDS area and point analyses result. Points 1 and 2 were determined as Mo_5Si_3 and Mo_3Si, respectively.

Figure 2 shows the morphology of the powders before and after spheroidizing by inductively coupled thermal plasma treatment. As shown in Figure 2a, the powders after milling and sieving had an irregular shape. The powder size distribution of the powder after milling was examined by a powder analyzer; the d_{10}, d_{50}, and d_{90} values were 47.9, 75.4, and 117.0 μm, respectively. Mo silicides, including Mo_5Si_3, have a brittle nature; grain boundary cracking occurs easily at room temperature [12]. Chu et al. [19] researched this by fabricating single crystal Mo_5Si_3 by the Czochralski method and evaluating the mechanical properties with respect to crystal orientation. The room temperature fracture toughness, which ranged from 2 to 2.5 MPa$\sqrt{m}$, was not severely affected by the crystal orientation. Therefore, the Mo_5Si_3 ingot was easily pulverized by jaw crushing and ball milling.

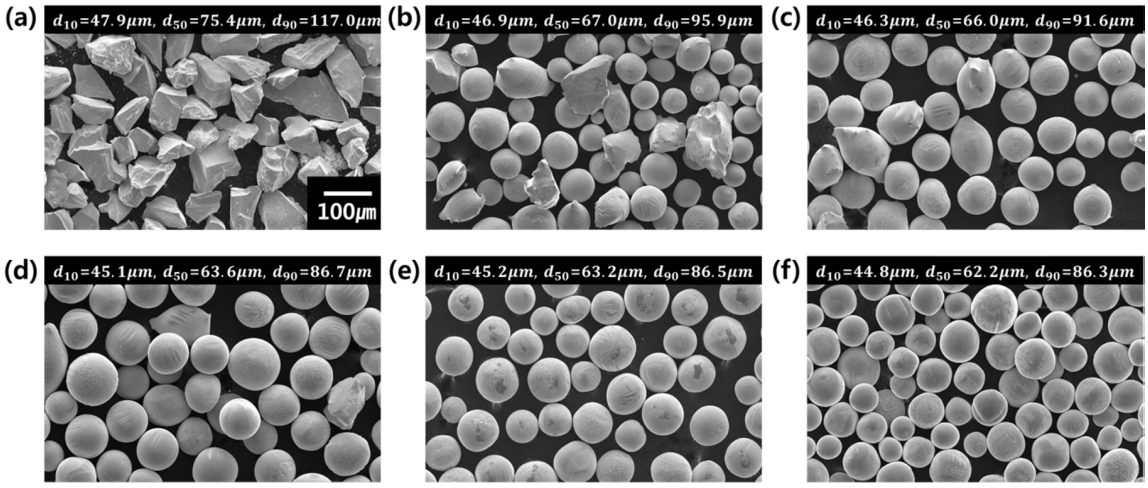

Figure 2. Morphology of the powders (**a**) after ball-milling and sieving, and (**b**–**f**) after spheroidizing by inductively coupled thermal plasma, with plasma powers of (**b**) 3 kW, (**c**) 4 kW, (**d**) 5 kW, (**e**) 6 kW, and (**f**) 7 kW.

After spheroidizing, the shape of the powders had changed from irregular to spherical. The sphericity of the powders was higher with increased plasma power. The powder size tended

to become smaller with increasing plasma power, and the d_{10}, d_{50}, and d_{90} values of the powder spheroidized at 7 kW were 44.8, 62.2, and 86.3 μm, respectively.

Previously, the temperature profile during inductively coupled thermal plasma treatment was simulated by COMSOL Multiphysics. The simulation indicated that the maximum temperature of the chamber was almost 10,000 K during plasma processing [20,21] and the powder reached maximum temperature within 10 ms after injecting in the plasma chamber [22]. Therefore, when powders with an irregular shape are injected into the plasma chamber, they are fully melted and spheroidized to reduce the surface area.

To analyze the phases present, the powders were examined by XRD. Figure 3a shows the XRD patterns for 2θ = 25–75° of the powders before and after spheroidizing. The powders were composed of two phases, Mo_5Si_3 and Mo_3Si. To investigate the percentage of Mo_5Si_3 and Mo_3Si in the powders, the XRD patterns were analyzed by the Rietveld method, and the result is shown in Figure 3b. The percentages of Mo_5Si_3 and Mo_3Si in the powder before spheroidizing were 92.5% and 7.5%, respectively. As the plasma power increased, the percentage of Mo_5Si_3 was gradually decreased in the spheroidized powders, reaching a minimum of 63.1% with the power of 7 kW.

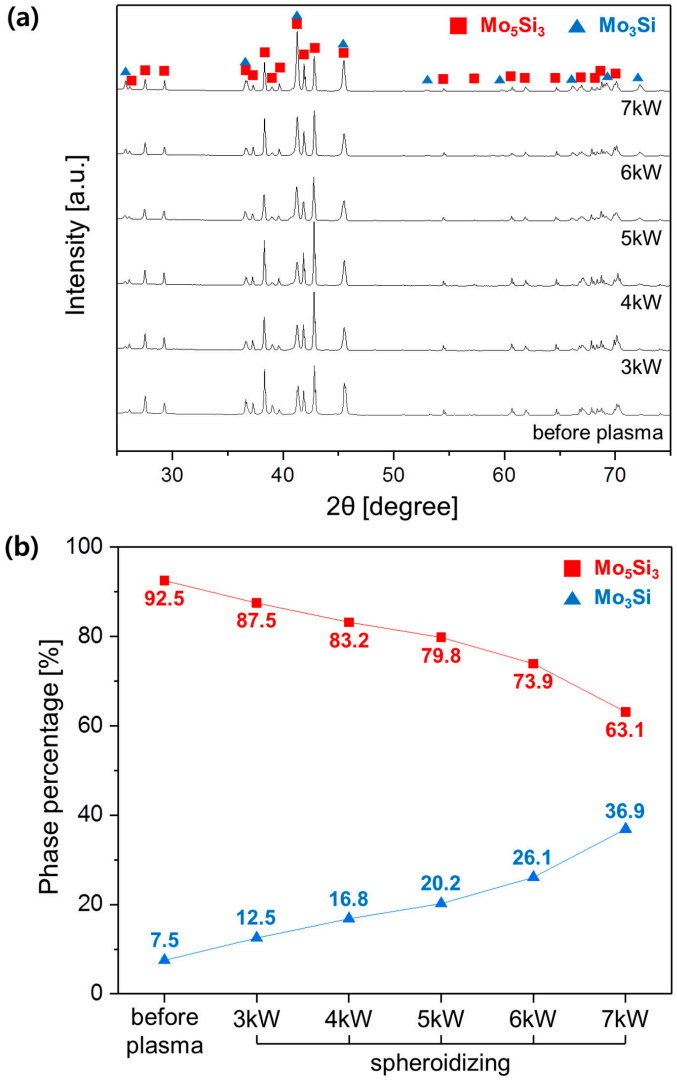

Figure 3. (**a**) XRD patterns of the powders before and after spheroidizing by inductively coupled thermal plasma treatment. (**b**) The percentage of each phase in the powders was analyzed by the Rietveld method based on the XRD data in Figure 3a.

By the chemical stoichiometry, the concentration of Si is greater in Mo_5Si_3 than in Mo_3Si (14.94 wt% vs. 8.89 wt%, respectively). The fact that the amount of the Si-rich phase reduces with increased plasma power suggests that Si evaporation may occur during plasma treatment. Therefore, the Si concentration of the powders was analyzed to examine this possibility.

Table 1 shows the Si concentration of the ingot and the powders after spheroidizing with different plasma powers. The weight concentration of Si in the Mo_5Si_3 having perfect stoichiometry is 14.94 wt%. The Si concentration of the ingot was 14.83 wt%, which is almost same as that of the Mo_5Si_3 phase. As the plasma power increased, the Si concentration gradually decreased, reaching a minimum of 11.15 wt% with the power of 7 kW. During the plasma treatment, the evaporation rate of Si would much higher than that of Mo; therefore, the Si concentration was decreased after spheroidizing.

The evaporation behavior of the element is determined by the vapor pressure [23,24]. An element with a higher vapor pressure will have a higher evaporation rate. The vapor pressure of a pure element i (p_i^o) is calculated by the following Equation [25]: $p_i^o = exp\left(-\frac{\Delta G_i^o}{RT}\right)$, where R is the gas constant, T is the temperature, and ΔG_i^o is the standard Gibbs free energy change of element i during the phase transformation from liquid to gas. Figure 4a shows the vapor pressure of pure Mo and Si with respect to the temperature. Both vapor pressures increase with increasing temperature. Furthermore, p_{Si}^o is higher than p_{Mo}^o over the whole temperature range, which means that the evaporation rate of Si is higher than that of Mo.

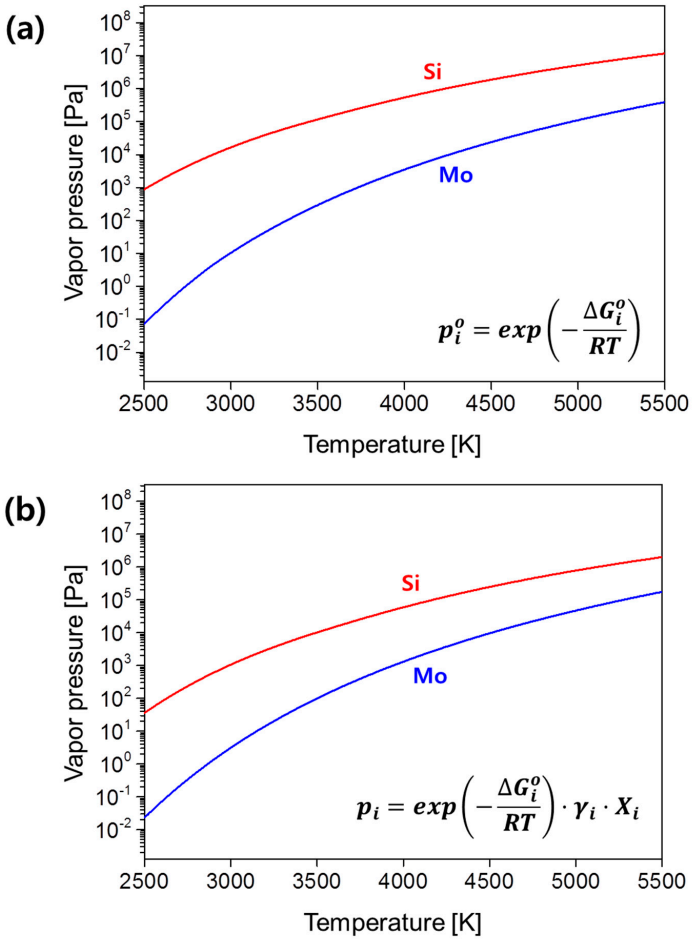

Figure 4. (**a**) Vapor pressure of pure Mo and Si with respect to temperature. (**b**) Vapor pressure of Mo and Si in molten Mo_5Si_3.

However, p_i^o is the vapor pressure for the pure element i. To more accurately analyze the evaporation behavior, the vapor pressures of Mo and Si in molten Mo_5Si_3 should be considered. The vapor pressure of element i in a liquid mixture (p_i) is calculated by the following equation: $p_i = exp\left(-\frac{\Delta G_i^o}{RT}\right) \cdot \gamma_i \cdot X_i$, where γ_i is the activity coefficient of element i in a liquid mixture and X_i is the molar fraction of element i [25]. To calculate the vapor pressure of Mo and Si in molten Mo_5Si_3 with respect to the temperature, activity coefficients of Mo and Si should be known. Therefore, the activity coefficients at 2500, 3000, 3500, 4000, 4500, 5000, and 5500 K of Mo and Si in the Mo–Si binary system were calculated by Thermo-Calc using the SSOL database. Then, the activity coefficients of Mo and Si in the composition of Mo_5Si_3 were extracted, and they were used to determine the p_{Mo} and p_{Si}.

Figure 4b shows the vapor pressures of Mo and Si in molten Mo_5Si_3 with respect to temperature. Since the evaporation rate in a liquid mixture is affected by the activity coefficient, the vapor pressures of Mo and Si in molten Mo_5Si_3 were different to that for pure Mo and Si. However, the vapor pressure of Si was still higher than that of Mo, confirming that the amount of Si evaporation was greater than that of Mo during plasma treatment. Therefore, the decreasing amount of the Si-rich phase (Mo_5Si_3) with increasing plasma power (Table 1) was caused by Si evaporation during spheroidizing. Even though Si was evaporated during spheroidizing, any condensation of Si was not observed. Si nanoparticles could be nucleated during plasma treatment; however, they would be filtered by the cyclone system due to their small size and low weight.

To determine the extent of oxygen contamination during the fabrication of the spherical Mo silicide powder, the oxygen concentrations of the ingot, the powders after milling, and the powders after spheroidizing at 6 kW were analyzed. The oxygen concentrations of the three samples are shown in Table 2. The oxygen concentration of the ingot was 0.003%, which increased to 0.171% after milling. This could be caused by the increase in specific surface area by pulverizing, as well as the contamination during milling, as argon purging may not perfectly eliminate oxygen from the milling container. After spheroidizing at 6 kW, the oxygen concentration was decreased to 0.016%. This would be due to the reducing environment during the plasma treatment, due to the extremely high temperature and low oxygen partial pressure in the chamber [21]. Thus, while the oxygen concentration was higher in the spheroidized powder than in the ingot, it was still considerably low.

To examine the internal microstructure of the spherical powder, the powder spheroidized at 6 kW was observed by FE-SEM. Figure 5a shows the cross-sectional microstructure of the powder observed by back-scattered electron imaging. As expected from the XRD results (Figure 3), the powders were composed of two phases. To identify the phases, EDS area and point analyses were performed, and the result is shown in Figure 5b. The Si concentrations of the dark area (Point 1) and bright area (Point 2) are 14.57 and 9.10 wt%, respectively. Therefore, the dark and bright areas can be defined as Mo_5Si_3 and Mo_3Si, respectively. The melting temperatures of Mo_5Si_3 and Mo_3Si are 2453 and 2298 K, respectively [26]. As the powders cooled during plasma treatment, the Mo_5Si_3 phase solidified first, after which Mo_3Si solidified. Therefore, the microstructure shown in Figure 5 would be formed by the first nucleation of Mo_5Si_3.

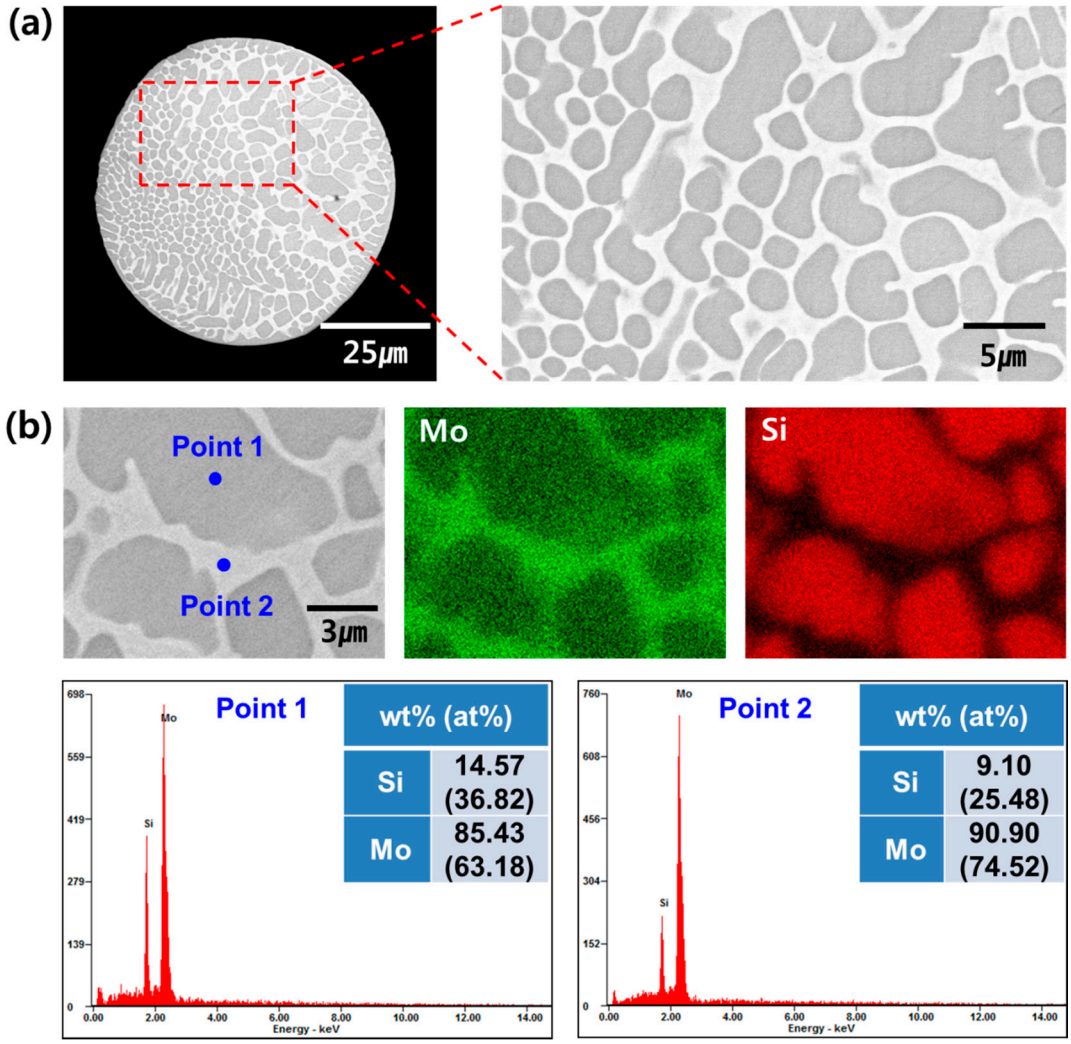

Figure 5. (**a**) Cross-sectional microstructure of the powder observed by back-scattered electron imaging, and (**b**) EDS area and point analyses result. Points 1 and 2 were determined as Mo_5Si_3 and Mo_3Si, respectively.

4. Conclusions

The Mo_5Si_3 ingot was prepared by vacuum arc melting, after which it was pulverized to a powder by jaw crushing and ball milling. As the milled powders had an irregular shape, they were spheroidized by thermal plasma treatment. As the plasma power increased, the sphericity of the powders increased. They were perfectly spheroidized when the plasma power was higher than 6 kW. After plasma treatment, the ratio of Mo_5Si_3 to Mo_3Si had decreased due to Si evaporation. Based on the thermodynamic analysis, Si has a higher vapor pressure than Mo in the Mo_5Si_3 liquid mixture. By this process, spherical Mo silicide powders with a low oxygen concentration of 0.016% could be fabricated successfully.

Author Contributions: Conceptualization, J.-W.K., J.M.P., B.-H.C. and S.L.; Data curation, K.B.P.; Formal analysis, J.M.P., J.H.P. and B.S.; Investigation, T.-W.N.; Methodology, H.K.K.; Writing original draft, H.-K. P.

Acknowledgments: This work was supported by a research fund of Korea Institute of Industrial Technology (KITECH EO-18-0012) and Agency for Defense Development (Project No. 811555-912515201).

Conflicts of Interest: The authors declare no conflict of interest.

References

1. Petrovic, J.J. $MoSi_2$-based high-temperature structural silicides. *MRS Bull.* **1993**, *18*, 35–41. [CrossRef]
2. Chu, F.; Thoma, D.J.; McClellan, K.J.; Peralta, P. Mo_5Si_3 single crystals: Physical properties and mechanical behavior. *Mater. Sci. Eng. A* **1999**, *261*, 44–52. [CrossRef]
3. Yeh, C.L.; Chou, C.C.; Hwang, P.W. Experimental and Numerical Studies on Self-Propagating High-Temperature Synthesis of Ta_5Si_3 Intermetallics. *Metals* **2015**, *5*, 1580–1590. [CrossRef]
4. Schneibel, J.H.; Liu, C.T.; Easton, D.S.; Carmichael, C.A. Microstructure and mechanical properties of Mo-Mo_3Si-Mo_5SiB_2 silicides. *Mater. Sci. Eng. A* **1999**, *261*, 78–83. [CrossRef]
5. Kwon, N.Y.; Kim, Y.D.; Suk, M.J.; Lee, S.; Oh, S.T. Synthesis of Mo-Si-B intermetallic compounds with continuous α-Mo matrix by pulverization of ingot and hydrogen reduction of MoO_3 powders. *Int. J. Refract. Met. Hard Mater.* **2017**, *65*, 25–28. [CrossRef]
6. Bewlay, B.P.; Jackson, M.R.; Zhao, J.C.; Subramanian, P.R. A review of very-high-temperature Nb-silicide-based composites. *Metall. Mater. Trans. A* **2003**, *34*, 2043–2052. [CrossRef]
7. Tang, Y.; Gua, X. High temperature deformation behavior of an optimized Nb-Si based ultrahigh temperature alloy. *Scr. Mater.* **2016**, *116*, 16–20. [CrossRef]
8. Byun, J.M.; Hwang, S.H.; Lee, S.; Kim, Y.D. Research trend of Mo based superalloys. *J. Kor. Powd. Met. Inst.* **2013**, *20*, 487–493. [CrossRef]
9. Kieffer, R.; Benesovsky, F. Recent developments in the field of silicides and borides of the high-melting-point transition metals. *Powder Metall.* **1958**, *1*, 145–171. [CrossRef]
10. Akinc, M.; Meyer, M.K.; Kramer, M.J.; Thom, A.J.; Huebsch, J.J.; Cook, B. Boron-doped molybdenum silicides for structural applications. *Mater. Sci. Eng. A* **1999**, *261*, 16–23. [CrossRef]
11. Choe, H.; Chen, D.; Schneibel, J.H.; Ritchie, R.O. Ambient to high temperature fracture toughness and fatigue-crack propagation behavior in a Mo–12Si–8.5B (at.%) intermetallic. *Intermetallics* **2001**, *9*, 319–329. [CrossRef]
12. Ström, E.; Zhang, J. Mechanical anisotropy and segregation in Mo_5Si_3 studied by EBSD. *Intermetallics* **2005**, *13*, 367–372. [CrossRef]
13. Mendiratta, M.G.; Dimiduk, D.M. Strength and toughness of a Nb/Nb_5Si_3 composite. *Metall. Mater. Trans. A* **1993**, *24*, 501–504. [CrossRef]
14. Zamani, S.; Bakhsheshi-Rad, H.R.; Shokuhfar, A.; Vaezi, M.R.; Kadir, M.R.A.; Shafiee, M.R.M. Synthesis and characterization of $MoSi_2$-Mo_5Si_3 nanocomposite by mechanical alloying and heat treatment. *Int. J. Refract. Met. Hard Mater.* **2012**, *31*, 236–241. [CrossRef]
15. Krüger, M.; Schmelzer, J.; Helmecke, M. Similarities and Differences in Mechanical Alloying Processes of V-Si-B and Mo-Si-B Powders. *Metals* **2016**, *6*, 241. [CrossRef]
16. Kermani, M.; Razavi, M.; Rahimipour, M.R.; Zakeri, M. The effect of mechanical alloying on microstructure and mechanical properties of $MoSi_2$ prepared by spark plasma sintering. *J. Alloy. Compd.* **2014**, *593*, 242–249. [CrossRef]
17. Fang, Z.Z.; Paramore, J.D.; Sun, P.; Chandran, K.S.R.; Zhang, Y.; Xia, Y.; Cao, F.; Koopman, M.; Free, M. Powder metallurgy of titanium—Past, present, and future. *Int. Mater. Rev.* **2017**. [CrossRef]
18. Danzaki, Y.; Wagatsuma, K.; Syoji, T.; Yoshimi, K. Dissolution of molybdenum-silicon (-boron) alloys using a mixture of sulfuric, nitric and hydrofluoric acids and a sequential correction method for ICP-AES analysis. *Fresen J. Anal. Chem.* **2001**, *369*, 184–186. [CrossRef]
19. Chu, F.; Thoma, D.J.; McClellan, K.; Peralta, P.; He, Y. Synthesis and properties of Mo_5Si_3 single crystals. *Intermetallics* **1999**, *7*, 611–620. [CrossRef]
20. Boulos, M.I. The role of transport phenomena and modeling in the development of thermal plasma technology. *Plasma Chem. Plasma Process.* **2016**, *36*, 3–28. [CrossRef]
21. Leparoux, M.; Loher, M.; Schreuders, C.; Siegmann, S. Neural network modelling of the inductively coupled RF plasma synthesis of silicon nanoparticles. *Powder Technol.* **2008**, *185*, 109–115. [CrossRef]
22. Tong, J.B.; Lu, X.; Liu, C.C.; Pi, Z.Q.; Zhang, R.J.; Qu, X.H. Numerical simulation and prediction of radio frequency inductively coupled plasma spheroidization. *Appl. Therm. Eng.* **2016**, *100*, 1198–1206. [CrossRef]
23. Chakrabarti, O.; Weisensel, L.; Sieber, H. Reactive melt infiltration processing of biomorphic Si–Mo–C ceramics from wood. *J. Am. Ceram. Soc.* **2005**, *88*, 1792–1798. [CrossRef]

24. Xu, L.; Huang, C.; Liu, H.; Zou, B.; Zhu, H.; Zhao, G.; Wang, J. Study on in-situ synthesis of ZrB_2 whiskers in ZrB_2–ZrC matrix powder for ceramic cutting tools. *Int. J. Refract. Met. Hard Mater.* **2013**, *37*, 98–105. [CrossRef]
25. Su, Y.; Guo, J.; Jia, J.; Liu, G.; L, Y. Composition control of a TiAl melt during the induction skull melting (ISM) process. *J. Alloy. Compd.* **2002**, *334*, 261–266.
26. Liu, Y.; Shao, G.; Tsakiropoulos, P. Thermodynamic reassessment of the Mo-Si and Al-Mo-Si system. *Intermetallics* **2000**, *8*, 953–962. [CrossRef]